Inorganic Chemistry

Article

pubs.acs.org/IC

$Na_2RE_2TeO_4(BO_3)_2$ (RE = Y, Dy−Lu): Luminescent and Structural Studies on a Series of Mixed Metal Borotellurates

Jiang-He Feng, Chun-Li Hu, Xiang Xu, Fang Kong, and Jiang-Gao Mao*

State Key Laboratory of Structural Chemistry, Fujian Institute of Research on the Structure of Matter, Chinese Academy of Sciences, Fuzhou 350002, P. R. China

Supporting Information

ABSTRACT: The first examples of metal borotellurates, namely, $Na_2RE_2TeO_4(BO_3)_2$ (RE = Y, Dy−Lu) have been prepared by using solid-state reactions. They possess similar structures and crystallize in space group $P2_1/c$ (No. 14). These compounds feature a novel $[RE_2TeO_4(BO_3)_2]^{2-}$ 3D network structure composed of linear $[TeO_4(BO_3)_2]^{8-}$ anions interconnected by RE^{3+} ions with the voids of the network filled by the Na^+ ions. They exhibit high thermal stability (higher than 800 °C). Results of magnetic measurements on Dy, Ho, and Er compounds indicate that they display weak antiferromagnetic interaction between RE(III) centers. Luminescent studies show that $Na_2Er_2TeO_4(BO_3)_2$ has a strong emission at 1.562 μm with a wide fwhm (70 nm) and moderate lifetime (0.18 ms), whereas $Na_2Yb_2TeO_4(BO_3)_2$ has a strong NIR region emission around 1.02 μm. Furthermore, UV−vis-NIR absorption spectra, infrared spectra, and DFT calculations for the Y compound as a representative were also accomplished.

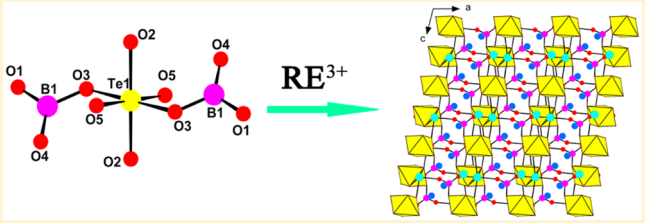

INTRODUCTION

Tremendous research attention has been devoted to metal borate research in recent decades due to their numerous structures and piquant physical properties, as well as their important applications in second-harmonic generation, photonic technologies, and catalysis.[1] So far, a number of excellent borate crystals have been widely used to convert the frequency of coherent laser sources, including β-BaB_2O_4 (β-BBO),[2] LiB_3O_5 (LBO),[3] CsB_3O_5 (CBO),[1d] $CsLiB_6O_{10}$ (CLBO),[4] and $KBe_2BO_3F_2$ (KBBF).[5] Boron can form a BO_3 planar triangle and a BO_4 tetrahedron, which can be further interlinked by corner-sharing or edge-sharing into various fundamental building blocks (FBBs), such as B_2O_5 B_3O_6, B_3O_7, and so forth.[6] These FBBs can generate many types of anionic structures that includes 1D chains, 2D layers, and 3D networks when they are bonded together.[7]

The combination of borates with oxoanions of the post-transition metal elements can further greatly enlarge the borate family to include borosilicates,[8] borogermanates,[9] borophosphates,[10] borosulfates,[11] and boroselenites,[12] among others. By combination of borates and selenites, a series of boroselenites including $Se_2B_2O_7$,[12a] $K_2Se_2B_2O_{10}$, $ASeB_3O_7$ (A = Na, K), and $Li_2SeB_8O_{15}$ have been obtained,[2] among which $Se_2B_2O_7$ displays a chiral 3D framework built of $B_2O_7^{8-}$ anions and SeO_3 groups and shows a moderate strong SHG signal. The borosulfates and borate-sulfate mixed anion compounds reported include $B_2S_2O_9$,[11a] $K_5[B(SO_4)_4]$,[11b] $Na_5[B(SO_4)_4]$, $Li[B(S_2O_7)_2]$, $A_3[B(SO_4)_3]$ (A = K, Rb),[11c] and $Pb_6O_2(BO_3)_2(SO_4)$.[11d] Intriguingly, $Li[B(SO_4)_2]$, $B_2S_2O_9$, and $K_5[B(SO_4)_4]$ belong to polar space groups. The crystal structure of $Li[B(SO_4)_2]$ exhibits a 3D network of corner-sharing BO_4 and SO_4 tetrahedra with Li^+ ions filling the voids of the framework. $B_2S_2O_9$ features a double-layered structure composed of corner-sharing BO_4 and SO_4 tetrahedra with six-member rings. $K_5[B(SO_4)_4]$ contains a 0D $[B(SO_4)_4]^{5-}$ anionic group made of a central BO_4 tetrahedron linking with four neighboring SO_4 tetrahedra.

Similar to selenium and sulfur, tellurium element can exhibit two oxidation states (+4 and +6). Te(IV) can form asymmetry TeO_3, TeO_4, and TeO_5 groups,[13] whereas Te(VI) cation favors an octahedral-geometry.[14] Numerous metal tellurites and tellurates have been documented, such as $BaTeM_2O_9$ (M = Mo^{6+} or W^{6+}),[15] $NaYTe_4O_{10}$,[16] $Ag_2Mo_3Te_3O_{16}$,[17] $Na_2M_2TeO_6$ (M = Ni^{2+}, Co^{2+}, Zn^{2+} or Mg^{2+}),[18] $BaMTe_2O_7$ (M = Mg^{2+}, Cu^{2+} or Zn^{2+}),[19] M_2GeTeO_6 (M = K^+, Rb^+ or Cs^+),[14b] among others. Based on the boroselenites, boro-sulfates reported, we believe that the combination of borate anion and tellurium(VI) or tellurium(IV) will lead to the formation of a new class of compounds with rich structure chemistry and interesting physical properties. Hitherto, no such compounds have been reported. Furthermore, in the fields of fluorescence and laser application, rare earth ions play an irreplaceable function for their unusual spectra characters.[20] Hence our efforts in the Na(I)-RE(III)-Te(VI)−B(III)−O system resulted in the isolation of the first examples of borotellurates, namely, $Na_2RE_2TeO_4(BO_3)_2$ (RE = Y, Dy−Lu). Herein, we present their syntheses, structural elucidation, luminescent, and magnetic properties.

Received: December 23, 2014
Published: February 18, 2015

DOI: 10.1021/ic503068s
Inorg. Chem. 2015, 54, 2447−2454

Table 1. Crystallographic Data and Structure Refinements for $Na_2RE_2TeO_4(BO_3)_2$ (RE = Y, Dy−Lu)[a]

formula	$Na_2Y_2TeBO_{10}$	$Na_2Dy_2TeBO_{10}$	$Na_2Ho_2TeBO_{10}$	$Na_2Er_2TeBO_{10}$	$Na_2Tm_2TeBO_{10}$	$Na_2Yb_2TeBO_{10}$	$Na_2Lu_2TeBO_{10}$
fw	533.02	680.20	685.06	689.72	693.06	701.28	705.14
space group	$P2_1/c$ (14)	$P2_1/c$ (14)	$P2_1/c$ (14)	$P2_1/c$ (14)	$P2_1/c$ (14)	$P2_1/c$ (14)	$P2_1/c$ (14)
a /Å	6.3073(7)	6.3089(5)	6.3060(5)	6.2964(5)	6.2801(4)	6.2631(6)	6.2588(5)
b/Å	9.9279(8)	9.9808(7)	9.9360(7)	9.9056(7)	9.8594(6)	9.8269(9)	9.7998(8)
c/ Å	6.7219(6)	6.7489(6)	6.7339(6)	6.7089(6)	6.6918(4)	6.6741(7)	6.6539(5)
β/deg	104.260(10)	104.394(8)	104.230(8)	104.110(8)	104.010(8)	103.972(10)	103.714(7)
vol/Å^3	407.94(7	411.62(6)	408.98(6)	405.81(6)	401.89(4)	398.62(7)	396.48(5)
Z	2	2	2	2	2	2	2
D_{calc}, g/cm^{-3}	4.339	5.488	5.563	5.645	5.727	5.843	5.907
μ,mm^{-1}	17.811	21.636	22.852	24.214	25.644	27.059	28.516
GOF on F^2	1.030	1.041	1.042	0.988	1.035	1.047	1.063
R_1, wR_2 [$I > 2\sigma(I)$]	0.0294, 0.0686	0.0359, 0.0834	0.0278, 0.0548	0.0273, 0.0568	0.0221, 0.0425	0.0373 0.0828	0.0314, 0.0731
R_1, wR_2 (all data)	0.0320, 0.0704	0.0423 0.0896	0.0353, 0.0605	0.0337, 0.0609	0.0285, 0.0452	0.0477, 0.0911	0.0373, 0.0784

[a] $R_1 = \sum||F_o| - |Fc||/\sum|F_o|$, $wR_2 = \{\sum w[(F_o)^2 - (F_c)^2]^2/\sum w[(F_o)^2]^2\}^{1/2}$

Table 2. Important Bond Lengths (angstroms) for $Na_2RE_2TeO_4(BO_3)_2$ (RE = Y, Dy−Lu)[a]

	Y	Dy	Ho	Er	Tm	Yb	Lu
RE(1)−O(1)	2.193(4)	2.213(8)	2.206(6)	2.174(7)	2.174(6)	2.175(8)	2.148(8)
RE(1)−O(2)#1	2.287(4)	2.293(7)	2.285(6)	2.267(6)	2.259(4)	2.253(9)	2.234(7)
RE(1)−O(4)	2.282(4)	2.298(7)	2.293(6)	2.277(7)	2.258(5)	2.250(9)	2.239(8)
RE(1)−O(5)#2	2.314(3)	2.323(7)	2.311(6)	2.306(6)	2.288(5)	2.278(9)	2.268(7)
RE(1)−O(4)#3	2.337(4)	2.353(7)	2.328(7)	2.333(6)	2.312(5)	2.300(8)	2.294(7)
RE(1)−O(2)	2.345(4)	2.373(7)	2.339(7)	2.346(5)	2.331(5)	2.322(8)	2.308(8)
RE(1)−O(5)#4	2.455(4)	2.470(7)	2.457(7)	2.440(6)	2.437(5)	2.428(8)	2.432(8)
Te(1)−O(5)	1.897(4)	1.894(7)	1.894(7)	1.893(6)	1.893(5)	1.901(8)	1.897(8)
Te(1)−O(5)#4	1.897(4)	1.894(7)	1.894(7)	1.893(6)	1.893(5)	1.901(8)	1.897(8)
Te(1)−O(2)#4	1.902(3)	1.912(6)	1.917(6)	1.908(6)	1.903(5)	1.905(9)	1.918(7)
Te(1)−O(2)	1.902(3)	1.912(6)	1.917(6)	1.908(6)	1.909(5)	1.905(9)	1.918(7)
Te(1)−O(3)#4	1.979(4)	1.978(8)	1.974(6)	1.966(6)	1.979(5)	1.982(9)	1.967(7)
Te(1)−O(3)	1.979(4)	1.978(8)	1.974(6)	1.966(6)	1.979(5)	1.982(9)	1.967(7)
B(1)−O(3)	1.407(7)	1.415(13)	1.414(12)	1.424(11)	1.419(8)	1.402(16)	1.418(14)
B(1)−O(1)#5	1.346(8)	1.321(14)	1.337(12)	1.344(12)	1.344(10)	1.325(17)	1.349(15)
B(1)−O(4)#6	1.373(8)	1.364(14)	1.355(13)	1.360(12)	1.364(10)	1.368(16)	1.374(15)

[a] Symmetry transformations used to generate equivalent atoms: #1 $x, -y + 3/2, z - 1/2$; #2 $-x, y + 1/2, -z + 1/2$; #3 $-x, -y + 2, -z$; #4 $x,-y + 1,-z$; #5 $-x + 1, y - 1/2, -z + 1/2$; #6 $-x, y - 1/2,-z + 1/2$.

EXPERIMENTAL SECTION

Materials and Methods. H_3BO_3 (99.9%), $NaCO_3$ (99.0%), and RE_2O_3 (99.9%) were acquired from Shanghai Reagent Factory, TeO_2 (Zhen Cui new material, 99.99%). Microprobe elemental analyses of elements Na, RE, and Te were accomplished on a field-emission scanning electron microscope (JSM6700F) equipped with an energy-dispersive X-ray spectroscope (EDS, Oxford INCA). Powder X-ray diffraction (PXRD) patterns were recorded on a XPERT-MPD θ-2θ diffractometer by graphite-monochromated Cu Kα radiation within 10−55° 2θ range with a step size of 0.05°. All thermogravimetric tests were performed by a NETZSCH STA 449F3 unit in air at 10 °C/min heating rate. All room-temperature optical diffuse reflectance spectra were tested on a PE Lambda 900 UV−vis spectrophotometer. We used $BaSO_4$ plate as a standard. All room-temperature absorption spectra were speculated from reflectance spectra through the Kubelka−Munk function.[21] Room-temperature photoluminescence studies and the relevant lifetime decay curves were accomplished on Edinburgh FLS920 and FSP920 fluorescence spectrometer. Magnetic susceptibility tests were accomplished with a PPMS-9T magnetometer in 2−300 K temperature range at 1000 Oe field.

Preparations of $Na_2RE_2TeO_4(BO_3)_2$ (RE = Y, Dy−Lu). All compounds were synthesized via traditional solid state reaction. The reaction mixtures composed of $NaCO_3$ (0.2120 g, 2.0 mmol), TeO_2 (0.6384 g, 4.0 mmol), H_3BO_3 (0.2473 g, 4.0 mmol), and RE_2O_3 (1.0 mmol) (RE = Y, Dy−Lu) were blended in agate mortars before been emptied into platinum crucibles. The mixtures were heated to 830 °C in 10 h, retained for 2 days, and then cooled to 600 °C at 3−5 °C/h rate; thereafter, the mixtures were cooled to room temperature at rate of 20 °C/h before quenching the furnace. As a representative, EDS elemental analyses of the Y phase showed an average Na/Y/Te molar ratio of 2.1/2.02/1.0, which agrees with the result from single-crystal X-ray diffraction analysis. Because structures were solved correctly, the polycrystalline samples of $Na_2RE_2TeO_4(BO_3)_2$ (RE = Y, Dy−Lu) were acquired quantitatively by reactions of a mixture of Na_2CO_3, TeO_2, H_3BO_3, and RE_2O_3 at a stoichiometric ratio at 800 °C for 3 days with intermittent regrinding. In the process of the reactions, Te^{4+} was oxidized to Te^{6+} by oxygen, such oxidation reactions have also been reported during the syntheses of $Na_2M_2TeO_6$ (M = Ni^{2+}, Co^{2+}, Zn^{2+} or Mg^{2+}).[16] Their purities were established through PXRD analysis (Figure S1). Attempts to obtain the Gd and Tb analogues were unsuccessful probably due to their larger ionic sizes.

Crystal Structure Determination. The single crystals of $Na_2RE_2TeO_4(BO_3)_2$ (RE = Y, Dy−Lu) were mounted on glass fibers for data collections using SuperNova with (Mo) X-ray Source, Mo Kα radiation (λ = 0.71073 Å) at room temperature. The data sets were corrected by the multiscan method for Lorentz and polarization factors as well as for absorption.[22] All seven crystal structures were determined using direct methods and refined with a full-matrix least-squares fitting on F^2 by SHELX−97.[23] PLATON was used to check for missing symmetry elements,[24] but none was found. Crystallographic data and structural refinements of $Na_2RE_2TeO_4(BO_3)_2$ (RE = Y, Dy−

DOI: 10.1021/ic503068s
Inorg. Chem. 2015, 54, 2447−2454

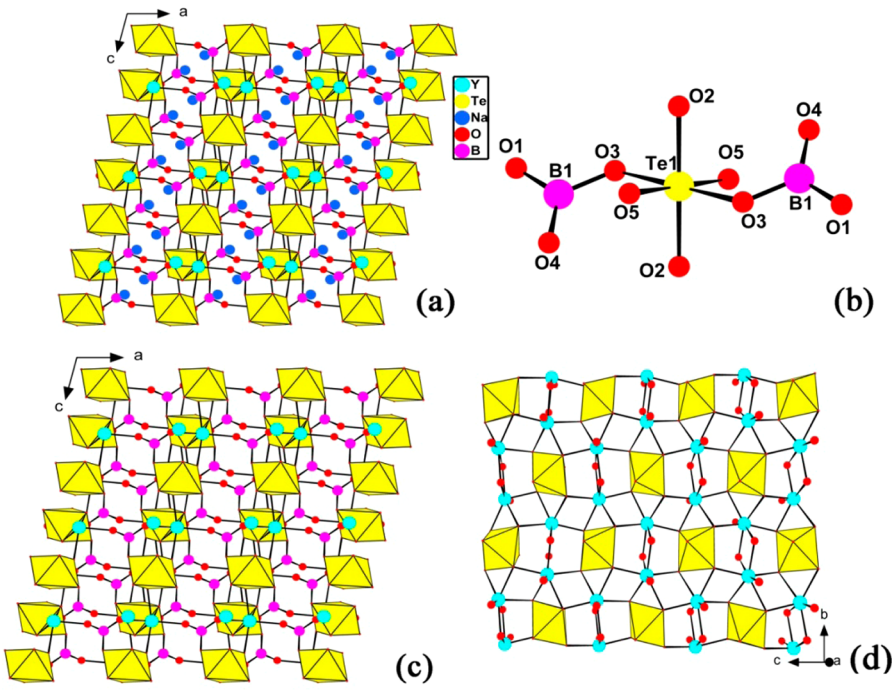

Figure 1. View of 3D structure of $Na_2Y_2TeO_4(BO_3)_2$ down the *b* axis (a), a $[TeO_4(BO_3)_2]^{8-}$ anion (b), 3D network of $[Y_2TeO_4(BO_3)_2]^{2-}$ (c), and 2D anionic layer of $[Y_2TeO_{10}]^{8-}$ in *bc*-plane (d).

Lu) are listed in Table 1, whereas the important bond distances are collected in Table 2. In terms of the study of crystallographic, details are displayed in the Supporting Information.

Computational Descriptions. Single crystal structural data of $Na_2Y_2TeO_4(BO_3)_2$ were taken as representative for calculation. The electronic structures and optical properties were calculated by DFT method within CASTEP program.[25] For the exchange-correlation function, we used the generalized-gradient-approximation and Perdew–Burke–Ernzerhof (DFT-GGA-PBE).[26] The norm-conserving pseudopotential were adopted to treat the core–electron interactions.[27] The Te-$5s^25p^4$, Y-$4d^15s^2$, Na-$2s^22p^63s^1$, B-$2s^22p^1$, O-$2s^22p^4$ valence electrons were considered. A cutoff energy of 750 eV and a k-point sampling of 4 × 3 × 4 were used in our calculation for $Na_2Y_2TeO_4(BO_3)_2$. The dielectric function $\varepsilon(\omega)$, from which the refractive indices can be obtained through $n^2(\omega = \varepsilon(\omega)$, was calculated according to the previously reported formula.[28]

RESULTS AND DISCUSSION

Crystal Structure. Our synthetic efforts in the Na(I)–RE(III)–Te(VI)–B(III)–O system resulted in the isolation of the first examples of borotellurates, namely, $Na_2RE_2TeO_4(BO_3)_2$ (RE = Y, Dy–Lu). They belong to a new structure type. These compounds are isostructural, hence we have chosen yttrium phase to discuss exhaustively as a representative of others. $Na_2Y_2TeO_4(BO_3)_2$ can be classified among the monoclinic $P2_1/c$ space group. The structure possesses a unique 3D anionic framework composed of linear $[TeO_4(BO_3)_2]^{8-}$ anions interconnected by Y^{3+} ions with the voids of the network filled by Na^+ cations (Figure 1a). Each symmetric unit of $Na_2Y_2TeO_4(BO_3)_2$ is made up of monatomic Te, Y, B, Na atoms and five O atoms. The Te^{6+} ion lies on an inversion center in comparison with that all other atoms locate at the general positions. In this structure, B atom is three-coordinated by three O atoms in a planar triangular geometry. The B–O distances locate between 1.344(8) to 1.407(7) Å and the O–B–O angles fall in the region from 117.5(5)° to 122.4 (5)°. All of them are compatible with other documented borates.[1d,4] Te atom is in a slightly distorted octahedral-geometry coordinated by six O atoms. The Te–O distances locate in the normal extent of 1.897(4)–1.979(4) Å and O–Te–O bond angles lie between 85.4(2)°–94.6(2)° for the *cis* O–Te–O and 180.0 for the *trans* O–Te–O, respectively. The above angles and distances are in agreement with those described in other metal tellurates.[18,29] The Y^{3+} ion is hepta-coordinated by seven oxygen atoms possessing Y–O bond lengths of 2.193(4)–2.455(4) Å. The geometry of the YO_7 polyhedron can be depicted as a monocapped trigonal prism. Na atom is in a distorted square antiprismatic geometry surrounded by eight oxygen atoms. Each Na–O distance is traceable between 2.307(4) to 2.919(5) Å. Bond valence calculations reveal that Na, Y, B, and Te correspond to the oxidation states of +1, +3, +3 and +6, respectively.[30] Furthermore, the calculated total bond valences of Na, Y, B, and Te are 0.992, 3.172, 2.986, and 5.919, respectively.

Each TeO_6 unit connects with two BO_3 groups to form linear 0D $[TeO_4(BO_3)_2]^{8-}$ borotellurate anion via corner-sharing (Figure 1b). These borotellurate anions are connected by Y^{3+} ions *into a 3D* $[Y_2TeO_4(BO_3)_2]^{2-}$ anionic network (Figure 1c). Each $[TeO_4(BO_3)_2]^{8-}$ anion connects with eight Y^{3+} ions. It is pertinent to note that the polyhedral of YO_7 are interlinked by edge-sharing to form a 2D yttrium oxide layer along *bc* plane, forming six-member rings occupied by Te^{6+} cations (Figure 1d). The Y···Y separations between two edge sharing YO_7 polyhedra are 3.647(8) and 3.749(8) Å, respectively. Hence the 3D network structure of the $[Y_2TeO_4(BO_3)_2]^{2-}$ anion can alternatively be described as formed by the 2D yttrium tellurate layers being interconnected by bridging BO_3 groups via B–O–Te bridges.

Owing to "lanthanide contraction", the RE–O bonds decrease slightly from Dy to Lu (Table 2). Accordingly, the cell volume also constricts by 3.70% from Dy to Lu (Table 1). However, this cause has very little effect on the distances of Te–O and B–O bonds (Table 2).

DOI: 10.1021/ic503068s
Inorg. Chem. 2015, 54, 2447–2454

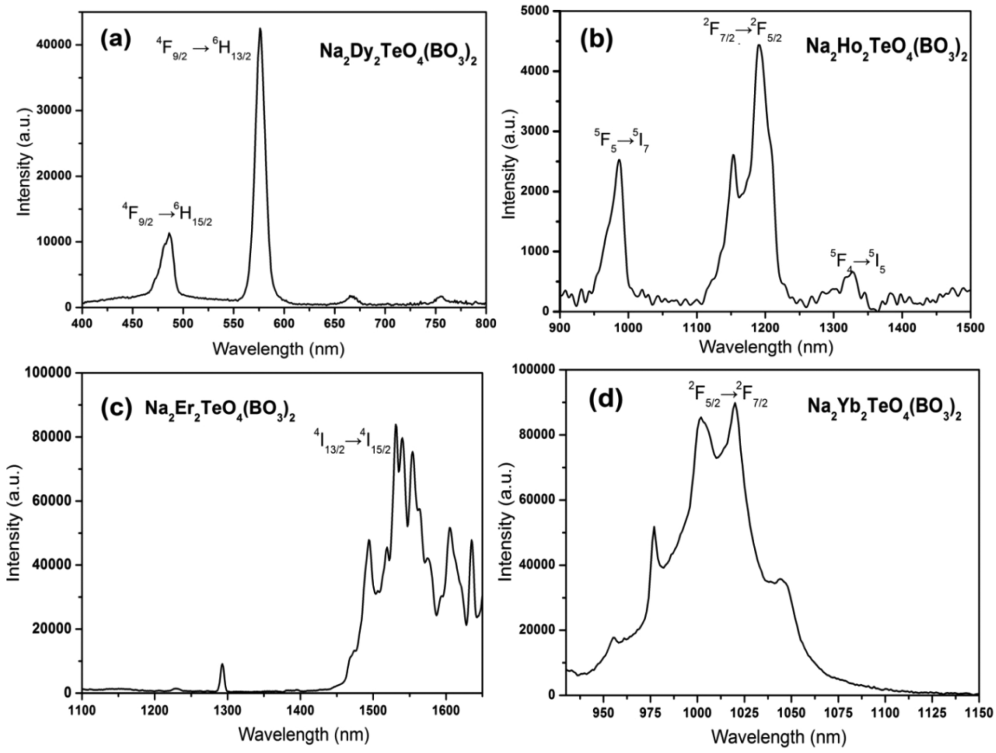

Figure 2. Solid state emission spectra of $Dy_2TeO_4(BO_3)_2$ (λ_{ex}= 353 nm) (a), $Na_2Ho_2TeO_4(BO_3)_2$ (λ_{ex} = 450 nm) (b), $Na_2Er_2TeO_4(BO_3)_2$ (λ_{ex} = 976 nm) (c), and $Na_2Yb_2TeO_4(BO_3)_2$ (λ_{ex} = 917 nm) (d).

It is intriguing comparing the structure of $Na_2Y_2TeO_4(BO_3)_2$ with that of $NaYTe_4O_{10}$ which exhibits a highly symmetric three-dimensional (3D) framework consisting of YO_8 square antiprisms and $[Te_2O_5]^{2-}$ dimers (The Te−O bond of 2.514(2) Å is excluded).[16] Within the framework, six- (6-) and eight-membered ring (8-MR) channels are observed. The lone pair active Te^{4+} cation in $NaYTe_4O_{10}$ is coordinated by three oxygens, whereas the Te^{6+} cation in $Na_2Y_2TeO_4(BO_3)_2$ is in an octahedral-geometry coordinated by six O atoms. Furthermore, $NaYTe_4O_{10}$ displays much larger anionic tunnels than those in $Na_2Y_2TeO_4(BO_3)_2$. Hence the inclusion of B atoms and the higher oxidation state of Te^{6+} have a great impact on the formation of material structures.

TGA and DSC Studies. The analysis of TGA illustrates that $Na_2RE_2TeO_4(BO_3)_2$ (RE = Y, Dy−Lu) compounds show slightly higher stable temperature with the increase of the lanthanide atomic number. They are stable up to 839.4, 842.1, 844.2 and 850.5, 852.0, 871.0, and 878.5 °C for Y, Dy−Lu, respectively (Figure S2 in the SI). Upon further heating, these compounds started to decompose and lose weight (2.70% for Y, 2.11% for Dy, 2.10% for Ho, 2.09% for Er, 2.08% for Tm, 2.05% for Yb, and 2.04% for Lu). These weight lost can be attributed to the release of some TeO_3, which is consistent with the endothermic peaks in DSC curves. The X-ray diffraction patterns of the $Na_2Y_2TeO_4(BO_3)_2$ after heating at 900 °C for 1 day demonstrate that the final residuals comprise $Na_2Y_2B_2O_7$, $Na_2Te_2O_7$, $Na_2B_8O_{13}$, and some other unknown compounds (Figure S3 in the SI).

Optical Properties. The study of optical diffuse reflectance spectra showcases that $Na_2RE_2TeO_4(BO_3)_2$ (RE = Y, Dy−Lu) can be classified among wide optical band gap semiconductors possessing band gaps of 3.52, 3.53, 3.56, 3.59, 3.68, 3.84, and 3.90 eV for Y, Dy−Lu compounds, respectively (Figure S4 in the SI). It is obvious that their band gaps increase slightly as the atomic number for the lanthanide ions increase.

The UV−vis−NIR absorption spectra of $Na_2RE_2TeO_4(BO_3)_2$ (RE = Dy−Tm) indicate that all the compounds have strong absorption peaks located between 300−2000 nm (Figure S5 in the SI). $Na_2Dy_2TeO_4(BO_3)_2$ shows sharp absorption bands at 455, 750, 800, 900, 1094, 1310, and 1672 nm. $Na_2Ho_2TeO_4(BO_3)_2$ exhibits sharp absorption bands at 363, 420, 450, 540, 640, 1157, and 1955 nm. $Na_2Er_2TeO_4(BO_3)_2$ also displays absorption bands at 380, 480, 520, 655, 799, 980, and 1500 nm. The absorption spectra of $Na_2Yb_2TeO_4(BO_3)_2$ compound displays two strong absorption bands at 917 and 976 nm. $Na_2Tm_2TeO_4(BO_3)_2$ shows absorption bands at 462, 689, 786, 1209, and 1264 nm. The f−f or f−d typical transitions of the respective lanthanide (III) ions result in these absorption peaks.[31]

The IR spectra of the seven compounds are exactly the same in peak positions, and therefore, we discuss the Y phase as a representative in detail. $Na_2Y_2TeO_4(BO_3)_2$ is transparent in 4000−1500 cm^{-1} (2.50−6.67 μm) range (Figure S6 in the SI). The IR absorption peaks (cm^{-1}) of $Na_2YTeO_4(BO_3)_2$ show the ν_{as}(B−O) at 1350 and 1220 cm^{-1}; ν_s(B−O) at 1165 and 941 cm^{-1}; ν_b(B−O) at 610 cm^{-1}; ν_s(Te−O) at 775, 720, and 650 cm^{-1}, and ν(Te−O antistretching and Te−O−Te vibrations) at 488 and 432 cm^{-1} (Figure S6 in the SI). These assignments are in accordance with other metal borates and tellurates.[9a,19,29,32]

Photoluminescence Studies. Luminescent spectra of $Na_2RE_2TeO_4(BO_3)_2$ (RE = Dy−Yb) were studied at room temperature. $Na_2Dy_2TeO_4(BO_3)_2$ shows typical emission bands for the Dy(III) ion when excited at 353 nm (Figure 2a). These emission bands can be ascribed to the transition of $^4F_{9/2} \rightarrow {}^6H_J$ (J = 15/2, 13/2, 11/2 and 9/2) of Dy(III) ion: 486 nm ($^4F_{9/2} \rightarrow {}^6H_{15/2}$), 576 nm ($^4F_{9/2} \rightarrow {}^6H_{13/2}$), 667 nm ($^4F_{9/2} \rightarrow {}^6H_{11/2}$), and 757 nm ($^4F_{9/2} \rightarrow {}^6H_{9/2}$). The lifetime of the Dy ($^4F_{9/2}$)

DOI: 10.1021/ic503068s
Inorg. Chem. 2015, 54, 2447−2454

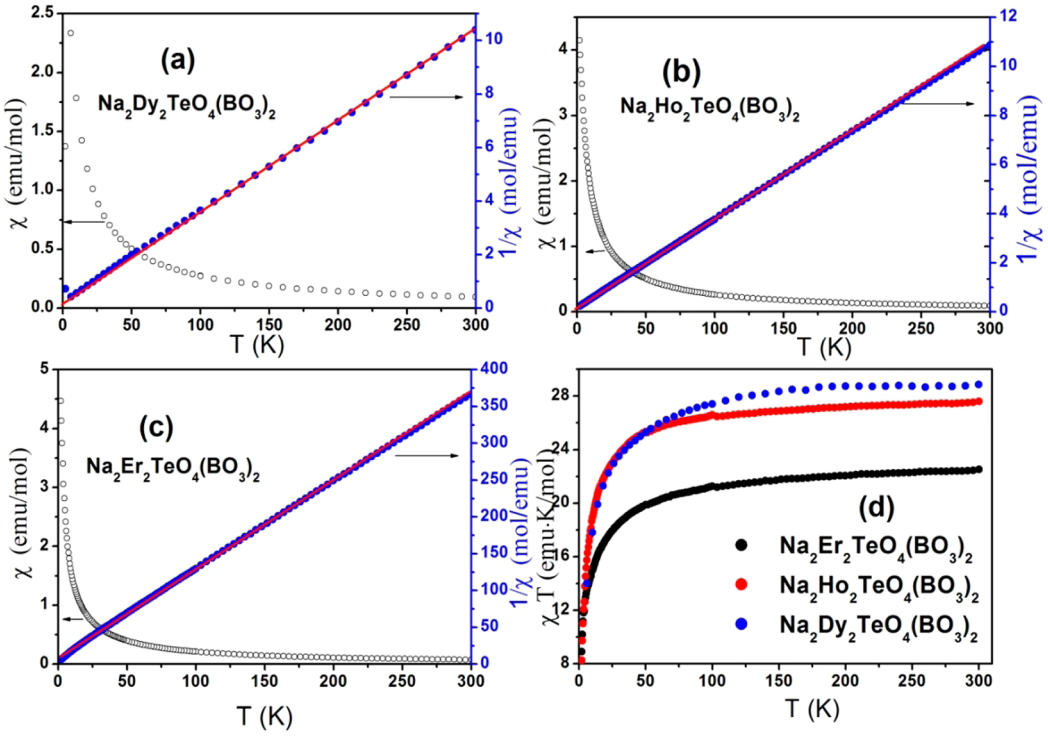

Figure 3. Plots of χ and $1/\chi$ *vs.* T for $Dy_2TeO_4(BO_3)_2$ (a), $Na_2Ho_2TeO_4(BO_3)_2$ (b) and $Na_2Er_2TeO_4(BO_3)_2$ (c), and the plots of χT vs T for three compounds (d). The red lines represent the linear fit of data according to the Curie–Weiss Law.

state for $\lambda_{ex,\,em}$ = 353, 576 nm was recorded to be 46.6 ns (Figure S7a in the SI). The short lifetime of the Dy ($^4F_{9/2}$) state is caused by fluorescence quenching effect of the high Dy(III) concentration. Figure 2b shows the room-temperature fluorescence spectra of $Na_2Ho_2TeO_4(BO_3)_2$ in the range of 1000–1500 nm when excited at 450 nm. There are two weak bands detected in the NIR region around 983 and 1189 nm, which can be assigned to $^5F_5 \rightarrow {}^5I_7$ and $^5I_6 \rightarrow {}^5I_8$ transitions, respectively. In addition, two other weak emission bands located at 1154 and 1328 nm are noticed, which probably arises from the splitting caused by crystal field.[33] Upon excitation at 976 nm, $Na_2Er_2TeO_4(BO_3)_2$ displays a wide emission band at 1.56 μm with full width at half-maximum (fwhm) of more than 70 nm (Figure 2c), which originates from $^4I_{13/2} \rightarrow {}^4I_{15/2}$ transitions of Er^{3+} ion. The splitting into several sub-bands originating from other transition bands indicates the influence of crystal field effect.[34] The lifetime of the Er ($^4I_{13/2}$) state for $\lambda_{ex,\,em}$ = 976, 1530 nm was measured to be 0.18 ms comparable with that in other crystals (Figure S7b in the SI).[30a,33] In addition, the laser output, around the wavelength of 1.55 μm, is situated in the region of "eye-safe" and matches the so-called third telecommunication window very well.[35] Furthermore, the large fwhm is greatly beneficial for the tunable laser output, so this compound is a potential 1.55 μm laser emission material. Excited at 917 nm, $Na_2Yb_2TeO_4(BO_3)_2$ possesses a strong NIR region emission at 1020 nm with fwhm more than 50 nm (Figure 2d), which originates from $^2F_{5/2} \rightarrow {}^2F_{7/2}$ transitions of the Yb^{3+} ion. The emission splits into four sub-bands, among which two strong peaks are of an interval of 20 nm (1000 and 1020 nm) that is in favor of the dual-wavelength laser output. The lifetime of the Yb ($^2F_{5/2}$) state for $\lambda_{ex,\,em}$ = 976, 1020 nm was measured to be 66.7 μs (Figure S7c in the SI).

Magnetic Properties. Magnetic properties of $Na_2RE_2TeO_4(BO_3)_2$ (RE = Dy–Er) have been determined in 2–300 K temperature range at 1000 Oe field. The temperature dependences of the corresponding reciprocal susceptibility ($1/\chi$) and the molar magnetic susceptibility (χ) are displayed in Figure 3. All three compounds fit the Curie–Weiss law. In temperature range of 2–300 K, the Curie constants C are 29.77, 27.92, and 0.83 cm^3 K mol^{-1} and Weiss temperatures θ are −8.55, −5.16, and −6.44 K for Dy, Ho, and Er compounds, respectively. The effective magnetic moments (μ_{eff}) per RE^{3+} ion at 300 K are calculated to be 10.75, 10.55, and 9.53 μ_B respectively for the Dy, Ho, and Er compounds. These calculated values are very approximate to their theoretical values of 10.63, 10.60, and 9.59 μ_B for Dy^{3+} ($^6H_{15/2}$, J = 15/2, g = 4/3), Ho^{3+} ($^5I_8$, J = 8, g = 5/4) and Er^{3+} ($^4I_{15/2}$, J = 15/2, g = 6/5), respectively. The small negative Weiss temperatures (θ) reveal that the antiferromagnetic interaction is weak between the magnetic ions in this type structure, due to the superexchange magnetic interactions between the RE^{3+} centers within the 2D rare earth oxide plane with a shortest RE···RE separation of 3.671(9), 3.657(9) and 3.644(8) Å for Dy, Ho and Er compounds, respectively. Because the Weiss temperature θ generally depends on the strongest coupling effect between the nearest magnetic centers (J). In a molecular field approximation, the coupling effect J between the RE^{3+} ions can be descried by $\theta = zJS(S + 1)/(3k_B)$,[36] where k_B is the Boltzmann constant and z depicts the number of nearest magnetic centers. We calculated out J = 1.349, 1.187, and 2.371 K with S = 2.5, 2, and 1.5 for Dy, Ho and Er compounds respectively, with z = 3, indicating that the antiferromagnetic interaction is extremely weak. The χT vs T plots in Figure 3d also illustrate that these compounds display weak antiferromagnetic properties. More specific magnetic interaction analysis was not carried out because of unavailability of suitable models available and its complex structure.

DOI: 10.1021/ic503068s
Inorg. Chem. 2015, 54, 2447–2454

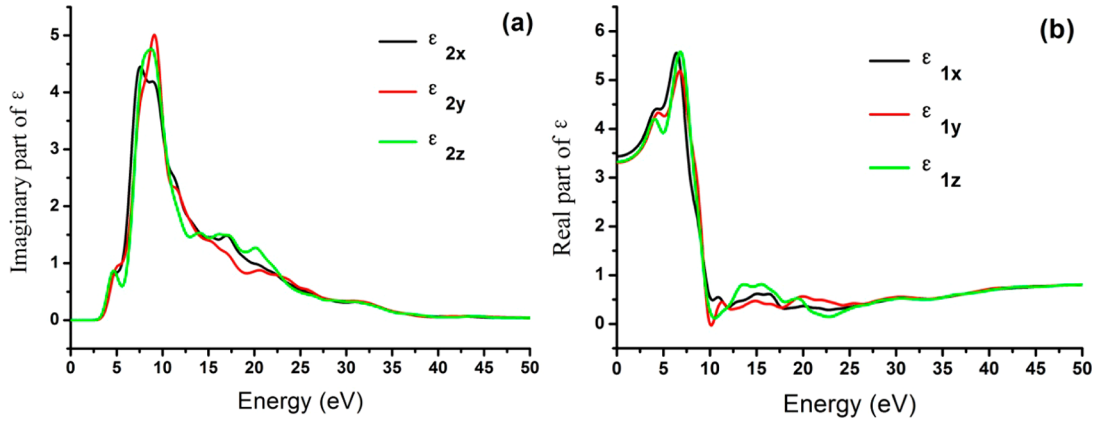

Figure 4. Calculated imaginary part (a) and the real part (b) of the dielectric function polarized along three dielectric axes directions for $Na_2YTeO_4(BO_3)_2$.

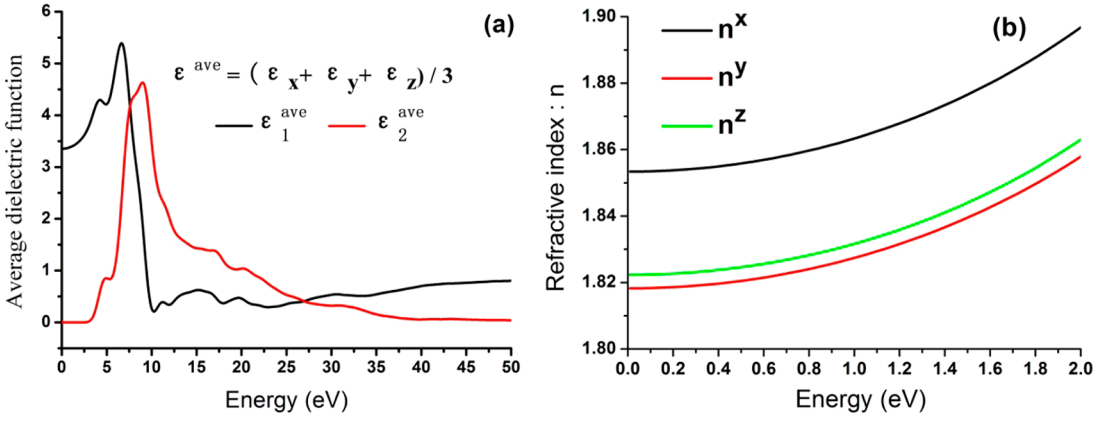

Figure 5. Calculated average imaginary part and real part of the dielectric function over three dielectric axes directions (a) and refractive indices (b) for $Na_2YTeO_4(BO_3)_2$.

Theoretical Studies. Because $Na_2RE_2TeO_4(BO_3)_2$ (RE = Y, Dy−Lu) compounds are isostructural, $Na_2Y_2TeO_4(BO_3)_2$ was adopted as a representative to describe the theoretical results. For the compound, the band structure is shown in Figure S8, and the state energies along special points in Brilluoin zone are listed in Table S1. For this compound, the valence band maximum (0.0 eV) is at C point, and the conduction band minimum (3.29677 eV) is at G point, indicating its indirect band gap characteristic. Its calculated band gap (3.30 eV) is smaller than that of experimentally measured value (3.52 eV), which results from the limitation of the exchange correlation function of GGA.[37]

The density of states (Figure S9) can be used to assign the bands in band structure. Obviously, the peak around −22.5 eV is from the very localized Na-2p states. The states in the range of −20 ∼ −15.5 eV mainly originate from O-2s, mixed by a few B-2s2p and Te-5s5p electronic states. The O-2p, B-2s2p, Y-4d and Te-5s5p states are all included over the two energy regions (−10−0 eV of valence band and 3−13 eV of conduction band), The full overlapping of electronic states in different atoms near the Fermi level shows the strong interactions of O with Te, B, and Y atoms in the system.

The population analyses (Table S2 in SI) indicate that the population of Y−O, Te−O and B−O bonds lie between 0.26−0.50, 0.47−0.52 and 0.74−0.95 e, respectively, the covalence characteristic has a trend of B−O > Te−O > Y−O. The Na−O bond order is small (0.01−0.12 e) due to their ionic bond nature.

Before studying the linear optical properties of $Na_2YTeO_4(BO_3)_2$, we need to determine the principal dielectric axis because of its monoclinic space group. Based on calculation according to the previously reported method,[38] for this crystal, the rotated angle of the coordinate axes of $a-c$ plane is −35.85°.

Figure 4 shows the imaginary and real parts dispersion curves of the dielectric function for $Na_2YTeO_4(BO_3)_2$, and both of them display strong anisotropy. The averaged dielectric function over different directions was also calculated (Figure 5a). The static dielectric constant is 3.35. The strongest absorption peak at 8.55 eV in $\varepsilon_2^{ave}(\omega)$ curve can be attributed to the transitions from the occupied O-2p to the unoccupied Y-4d, B-2p, and Te-5p states. The refractive indices can be obtained by $n^2(\omega = \varepsilon(\omega)$ and have the trend of $n^x > n^z > n^y$ during the energy range of 0−2 eV for the crystal (Figure 5b). The static n^x, n^y, and n^z (at 0.0 eV) values were calculated to be 1.85, 1.81, and 1.82, respectively.

CONCLUSIONS

The first examples of borotellurates, namely, $Na_2RE_2TeO_4(BO_3)_2$ (RE = Y, Dy−Lu), have been isolated using traditional solid state reaction. Structures of these compounds feature a novel $[RE_2TeO_4(BO_3)_2]^{2-}$ 3D network composed of linear $[TeO_4(BO_3)_2]^{8-}$ anions interconnected by

DOI: 10.1021/ic503068s
Inorg. Chem. 2015, 54, 2447−2454

RE^{3+} ions with the voids of the network filled by the Na^+ ions. All of them exhibit high thermal stability. $Na_2Er_2TeO_4(BO_3)_2$ displays a strong emission at 1.56 μm with a wide fwhm (70 nm) and moderate lifetime (0.18 ms, 976 nm-ex), whereas $Na_2Yb_2TeO_4(BO_3)_2$ has a strong NIR region emission at 1.02 μm with a wide fwhm (50 nm). Between magnetic centers, the Dy, Ho, and Er compounds all exhibit weak antiferromagnetic exchange interactions. We can anticipate that other new compounds which combine borate and tellurate or tellurite groups could be acquired by analogous synthetic methods.

■ ASSOCIATED CONTENT

Ⓢ Supporting Information

X-ray crystallographic files in CIF format, simulated and experimental XRD powder patterns, UV−vis−NIR absorption spectra, infrared spectra, band structure and DOS diagrams. This material is available free of charge via the Internet at http://pubs.acs.org.

■ AUTHOR INFORMATION

Corresponding Author

*E-mail: mjg@fjirsm.ac.cn. Fax: (+86)591-83704836.

Notes

The authors declare no competing financial interest.

■ ACKNOWLEDGMENTS

This work was supported by National Natural Science Foundation of China (Grants 21231006, 21373222, and 21401194).

■ REFERENCES

(1) (a) Wang, S. C.; Ye, N. *J. Am. Chem. Soc.* **2011**, *133*, 11458−11461. (b) Becker, P. *Adv. Mater.* **1998**, *10*, 979−992. (c) Chen, C. T.; Wang, Y. B.; Wu, B. C.; Wu, K. C.; Zeng, W. L.; Yu, L. H. *Nature* **1995**, *373*, 322−324. (d) Wu, Y. C.; Sasaki, T.; Nakai, S.; Yokotani, A.; Tang, H. G.; Chen, C. T. *Appl. Phys. Lett.* **1993**, *62*, 2614−2615. (e) Chen, C. T.; Liu, G. Z. *Annu. Rev. Mater. Sci.* **1986**, *16*, 203−243. (f) Chen, C. T.; Wu, B. C.; You, G. M.; Jiang, A. D.; Huang, Y. C. *J. Opt. Soc. Am. B* **1984**, *1*, 434−435.

(2) Chen, C. T.; Wu, B. C.; Jiang, A. D.; You, G. M. *Sci. Sin., Ser. B: Chem.* **1985**, *28*, 235−243.

(3) Chen, C. T.; Wu, Y. C.; Jiang, A. D.; Wu, B. C.; You, G. M.; Li, R. K.; Lin, S. J. *J. Opt. Soc. Am. B* **1989**, *6*, 616−621.

(4) Mori, Y.; Kuroda, I.; Nakajima, S.; Sasaki, T.; Nakai, S. *Appl. Phys. Lett.* **1995**, *67*, 1818−1820.

(5) Chen, C. T.; Wang, Y. B.; Xia, Y. N.; Wu, B. C.; Tang, D. Y.; Wu, K. C.; Zeng, W. R.; Yu, L. H.; Mei, L. F. *J. Appl. Phys.* **1995**, *77*, 2268−2272.

(6) Jin, S. F.; Cai, G. M.; Wang, W. Y.; He, M.; Wang, S. C.; Chen, X. L. *Angew. Chem., Int. Ed.* **2010**, *49*, 4967−4970.

(7) Touboul, M.; Penin, N.; Nowogrocki, G. *J. Solid State Chem.* **2003**, *5*, 1327−1342.

(8) Parise, J. B.; Gier, T. E. *Chem. Mater.* **1992**, *4*, 1065−1067.

(9) (a) Hao, Y. C.; Hu, C. L.; Xu, X.; Kong, F.; Mao, J. G. *Inorg. Chem.* **2013**, *52*, 13644−13650. (b) Li, Y. F.; Zou, X. D. *Angew. Chem., Int. Ed.* **2005**, *44*, 2012−2015.

(10) Kniep, R.; Gozel, G.; Eisenmann, B.; Rohr, C.; Asbrand, M.; Kizilyalli, M. *Angew. Chem., Int. Ed.* **1994**, *33*, 749−751.

(11) (a) Logemann, C.; Wickleder, M. S. *Angew. Chem., Int. Ed.* **2013**, *52*, 14229−14232. (b) Hoppe, H. A.; Kazmierczak, K.; Daub, M.; Forg, K.; Fuchs, F.; Hillebrecht, H. *Angew. Chem., Int. Et.* **2012**, *51*, 6255−6257. (c) Daub, M.; Kazmierczak, K.; Gross, P.; Hoppe, H.; Hillebrecht, H. *Inorg. Chem.* **2013**, *52*, 6011−6020. (d) Aurivillius, B. *Chem. Scripta.* **1983**, *22*, 168−170.

(12) (a) Kong, F.; Huang, S. P.; Sun, Z. M.; Mao, J. G.; Cheng, W. D. *J. Am. Chem. Soc.* **2006**, *128*, 7750−7751. (b) Zhang, J. H.; Kong, F.; Yang, B. P.; Mao, J. G. *CrystEngComm* **2012**, *14*, 8727−8733.

(13) (a) Becker, C. R.; Tagg, S. L.; Huffman, J. C.; Zwanziger, J. W. *Inorg. Chem.* **1997**, *36*, 5559−5564. (b) Ok, K. M.; Halasyamani, P. S. *Chem. Mater.* **2001**, *13*, 4278−4284.

(14) (a) Woodward, P. M.; Sleight, A. W.; Du, L. S.; Grey, C. P. *J. Solid State Chem.* **1999**, *147*, 99−116. (b) Amarilla, M.; Veiga, M. L.; Pico, C.; Gaitan, M.; Jerez, A. *Inorg. Chem.* **1989**, *28*, 1701−1703.

(15) Ra, H. S.; Ok, K. M.; Halasyamani, P. S. *J. Am. Chem. Soc.* **2003**, *125*, 7764−7765.

(16) Kim, Y. H.; Lee, D. W.; Ok, K. M. *Inorg. Chem.* **2015**, *54*, 389−395.

(17) Zhou, Y.; Hu, C. L.; Hu, T.; Kong, F.; Mao, J. G. *Dalton Trans.* **2009**, 5747−5754.

(18) Evstigneeva, M. A.; Nalbandyan, V. B.; Petrenko, A. A.; Medvedev, B. S.; Kataev, A. A. *Chem. Mater.* **2011**, *23*, 1174−1181.

(19) Yeon, J.; Kim, S. H.; Nguyen, S. D.; Lee, H.; Halasyamani, P. S. *Inorg. Chem.* **2012**, *51*, 2662−2668.

(20) (a) Taccheo, S.; Laporta, P.; Longhi, S.; Svelto, O.; Svelto, C. *Appl. Phys. B: Laser Opt.* **1996**, *63*, 425−3130. (b) Deloach, L. D.; Payne, S. A.; Chase, L. L.; Smith, L. K.; Kway, W. L.; Krupke, W. F. *IEEE J. Quantum. Elect.* **1993**, *29*, 1179−1191. (c) Jaque, D.; Capmany, J.; Luo, Z. D.; Sole, J. G. *J. Phys.: Condens. Matter* **1997**, *9*, 9715−9729. (d) Liu, B.; Kong, L.; Shi, C. *J. Lumin.* **2007**, *122*, 121−124.

(21) Wendlandt, W. M.; Hecht, H. G. *Reflectance Spectroscopy*; Interscience: New York, 1966.

(22) *CrystalClear*, version 1.3.5; Rigaku Corp.: Woodlands, TX, 1999.

(23) Sheldrick, G. M. *SHELXTL, Crystallographic Software Package*, version 5.1; Bruker-AXS: Madison, WI, 1998.

(24) Spek, A. L. *PLATON*; Utrecht University: Utrecht, The Netherlands, 2001.

(25) (a) Segall, M. D.; Lindan, P. J. D.; Probert, M. J.; Pickard, C. J.; Hasnip, P. J.; Clark, S. J.; Payne, M. C. *J. Phys-Condens Mater.* **2002**, *14*, 2717−2744. (b) Milman, V.; Winkler, B.; White, J. A.; Pickard, C. J.; Payne, M. C.; Akhmatskaya, E. V.; Nobes, R. H. *Int. J. Quantum Chem.* **2000**, *77*, 895−910.

(26) Perdew, J. P.; Burke, K.; Ernzerhof, M. *Phys. Rev. Lett.* **1996**, *77*, 3865−3868.

(27) Lin, J. S.; Qteish, A.; Payne, M. C.; Heine, V. *Phys. Rev. B* **1993**, *47*, 4174−4181.

(28) Bassani, F.; Parravicini, G. P. *Electronic States and Optical Transitions in Solids*; Pergamon Press Ltd.: Oxford, U.K., 1975.

(29) Porter, Y.; Ok, K. M.; Bhuvanesh, N. S. P.; Halasyamani, P. S. *Chem. Mater.* **2001**, *13*, 1910−1915.

(30) (a) Altermatt, D.; Brown, I. D. *Acta Crystallogr. B* **1985**, *41*, 240. (b) Brese, N. E.; Okeeffe, M. *Acta Crystallogr. B* **1991**, *47*, 192−197.

(31) (a) You, W. X.; Lin, Y. F.; Chen, Y. J.; Luo, Z. D.; Huang, Y. D. *Opt. Mater.* **2007**, *29*, 488−493. (b) Tang, J. F.; Chen, Y. J.; Lin, Y. F.; Gong, X. H.; Huang, J. H.; Luo, Z. D.; Huang, Y. D. *J. Phys. D: Appl. Phys.* **2010**, *43*, Article No. 495401. (c) Wang, Y.; You, Z. Y.; Li, J. F.; Zhu, Z. J.; Tu, C. Y. *J. Phys. D: Appl. Phys.* **2010**, *43*, Article No. 075402. (d) Ji, Y. X.; Cao, J. F.; Xu, J. L.; You, Z. Y.; Zhu, Z. J.; Li, J. F.; Wang, Y.; Tu, C. Y. *J. Alloy. Compd.* **2013**, *576*, 98−102. (e) Cao, J. F.; Ji, Y. X.; Li, J. F.; Zhu, Z. J.; Wang, Y.; You, Z. Y.; Tu, C. Y. *J. Lumin.* **2011**, *131*, 1350−1354.

(32) (a) Yang, Y.; Su, X.; Pan, S. L.; Zhang, M.; Wang, Y.; Han, J.; Yang, Z. H. *CrystEngComm* **2014**, *16*, 1978−1984. (b) Liu, L. L.; Su, X.; Yang, Y.; Pan, S. L.; Dong, X. Y.; Han, S. J.; Zhang, M.; Kang, J.; Yang, Z. H. *Dalton Trans.* **2014**, *43*, 8905−8918.

(33) Ji, Y. X.; Cao, J. F.; Zhu, Z. J.; Wang, Y.; Li, J. F.; You, Z. Y.; Tu, C. Y. *Mater. Res. Innov.* **2012**, *16*, 350−355.

(34) (a) Gong, X. H.; Lin, Y. F.; Chen, Y. J.; Liao, J. S.; Chen, X. Y.; Luo, Z. D.; Huang, Y. D. *Appl. Phys. B-Lasers O* **2008**, *91*, 499−505. (b) Lu, X. A.; You, Z. Y.; Li, J. F.; Zhu, Z. J.; Jia, G. H.; Wu, B. C.; Tu, C. Y. *J. Alloy. Compd.* **2006**, *426*, 352−356.

(35) (a) Kopczynski, K.; Mierczyk, Z.; Kaczmarek, S. *Laser Technology V: Physics and Research and Development Trends* **1997**,

DOI: 10.1021/ic503068s
Inorg. Chem. 2015, 54, 2447−2454

3186, 292−295. (b) Miniscalco, W. J. *J. Lightwave Technol.* **1991**, *9*, 234−250. (c) Wang, Q.; Dutta, N. K.; Ahrens, R. *J. Appl. Phys.* **2004**, *95*, 4025−4028.
(36) Bartlett, B. M.; Nocera, D. G. *J. Am. Chem. Soc.* **2005**, *127*, 8985−8993.
(37) (a) Okoye, C. M. I. *J. Phys.: Condens. Matter* **2003**, *15*, 5945−5958. (b) Godby, R. W.; Schluter, M.; Sham, L. J. *Phys. Rev. B* **1987**, *36*, 6497−6500.
(38) (a) Yang, B. P.; Hu, C. L.; Xu, X.; Sun, C. F.; Zhang, J. H.; Mao, J. G. *Chem. Mater.* **2010**, *22*, 1545−1550. (b) Sun, C. F.; Hu, C. L.; Xu, X.; Ling, J. B.; Hu, T.; Kong, F.; Long, X. F.; Mao, J. G. *J. Am. Chem. Soc.* **2009**, *131*, 9486−9487.

DOI: 10.1021/ic503068s
Inorg. Chem. 2015, 54, 2447−2454